Eur. J. Biochem. *230*, 1014–1024 (1995)

Rotational dynamics of calcium-free calmodulin studied by ^{15}N-NMR relaxation measurements

Nico TJANDRA[1], Hitoshi KUBONIWA[1], Hao REN[2] and Ad BAX[1]

[1] Laboratory of Chemical Physics, National Institute of Diabetes and Digestive and Kidney Diseases, National Institutes of Health, Bethesda MD, USA
[2] Laboratory of Biochemistry, National Cancer Institute, National Institutes of Health, Bethesda MD, USA

(Received 29 December 1994) – EJB 94 2021/3

The backbone motions of calcium-free *Xenopus* calmodulin have been characterized by measurements of the ^{15}N longitudinal relaxation times (T_1) at 51 and 61 MHz, and by conducting transverse relaxation (T_2), spin-locked transverse relaxation ($T_{1\rho}$), and ^{15}N-{^{1}H} heteronuclear NOE measurements at 61 MHz ^{15}N frequency. Although backbone amide hydrogen exchange experiments indicate that the N-terminal domain is more stable than calmodulin's C-terminal half, slowly exchanging backbone amide protons are found in all eight α-helices and in three of the four short β-strands. This confirms that the calcium-free form consists of stable secondary structure and does not adopt a 'molten globule' type of structure. However, the C-terminal domain of calmodulin is subject to conformational exchange on a time scale of about 350 μs, which affects many of the C-terminal domain residues. This results in significant shortening of the ^{15}N T_2 values relative to $T_{1\rho}$, whereas the $T_{1\rho}$ and T_2 values are of similar magnitude in the N-terminal half of the protein. A model in which the motion of the protein is assumed to be isotropic suggests a rotational correlation time for the protein of about 8 ns but quantitatively does not agree with the magnetic field dependence of the T_1 values and does not explain the different T_2 values found for different α-helices in the N-terminal domain. These latter parameters are compatible with a flexible dumbbell model in which each of calmodulin's two domains freely diffuse in a cone with a semi-angle of about 30° and a time constant of about 3 ns, whereas the overall rotation of the protein occurs on a much slower time scale of about 12 ns. The difference in the transverse relaxation rates observed between the amides in helices C and D suggests that the change in interhelical angle upon calcium binding is less than predicted by Herzberg et al. Strynadka and James [Strynadka, N. C. J. & James, M. N. G. (1988) *Proteins Struct. Funct. Genet. 3*, 1–17].

Keywords. Calmodulin; NMR; protein dynamics; ^{15}N relaxation; domain motion.

Calmodulin (CaM) is a ubiquitous 16.7-kDa intracellular protein of 148 residues that plays a key role in coupling Ca^{2+} transients, caused by a stimulus at the cell surface, to events in the cytosol (Cohen and Klee, 1988). It performs this role by binding to a host of intracellular enzymes in a calcium-dependent manner. In the crystalline state, Ca^{2+}-ligated calmodulin resembles a dumbbell, in which the small globular amino- and carboxy-terminal domains are linked by a 26-residue α-helix, frequently referred to as the 'central helix' (Babu et al., 1985, 1988; Taylor et al., 1991). However, ^{15}N-NMR relaxation experiments (Barbato et al., 1992) and small-angle X-ray scattering studies (Heidorn and Trewhella, 1988) both indicated that the helical linker, found in the crystalline state, is highly flexible in solution. Moreover, the NMR study unequivocally identified residues K77–S81, located near the middle of this 'central helix' as non-helical and highly flexible. The functional significance of the flexibility of the linker was shown in subsequent NMR and X-ray studies of Ca^{2+}-CaM structures complexed with peptide fragments of the binding sites of CaM-target enzymes: each of these complexes adopts a globular shape, in which the target peptide is clamped between the N- and C-terminal halves of CaM (Ikura et al., 1992; Meador et al., 1992, 1993).

No structure has been reported yet for Ca^{2+}-free CaM, although a model for its structure has been proposed (Strynadka and James, 1988) by analogy with a crystal structure of the homologous protein troponin C, in which the C-terminal domain is Ca^{2+}-ligated, whereas the N-terminal domain is not (Sundaralingam et al., 1985; Herzberg and James, 1988). Attempts to crystallize the Ca^{2+}-free form of CaM have been unsuccessful, but a recent NMR study of the C-terminal domain suggests a conformational change upon Ca^{2+} ligation which qualitatively confirms the Strynadka and James model (Finn et al., 1994). The spectral dispersion of the ^{1}H-^{15}N two-dimensional NMR spectrum is considerably worse compared to the Ca^{2+}-ligated form and exhibits severe line broadening for many of the backbone amide resonances. These observations have led to speculations that the Ca^{2+}-free state might not adopt a stable and well-defined structure, but instead might exist as a 'molten globule'. The present study provides evidence that Ca^{2+}-free CaM adopts a well-defined structure with a large fraction of its backbone amide protons significantly protected from exchange with the solvent. The backbone dynamics are also similar in nature to those observed previously for Ca^{2+}-ligated CaM (Barbato et al.,

Correspondence to A. Bax, Building 5, Room 126, National Institutes of Health, Bethesda, Maryland, MD 20892-0520, USA
Fax: +1 301 402 0907.

Abbreviations. CaM, calmodulin; HSQC, heteronuclear single-quantum correlation; T_1, longitudinal relaxation time; T_2, transverse relaxation time; $T_{1\rho}$, spin-locked transverse relaxation time; rms, root-mean-square.

1992), indicating that Ca^{2+}-free CaM also consists of two small globular domains, connected by a flexible linker.

^{15}N relaxation measurements of isotopically enriched proteins, using sensitive ^1H-detected two-dimensional experiments, have become an accepted procedure for characterizing overall protein motion, and for determining the degree of local backbone flexibility (Kay et al., 1989; Clore et al., 1990b; Szyperski et al., 1993; Schneider et al., 1992; Redfield et al., 1992; Akke et al., 1993; Torchia et al., 1993; Wagner et al., 1993; Palmer, 1993; van Mierlo et al., 1993; Peng and Wagner, 1992, 1994; Orekhov, 1994; Alexandrescu and Shortle, 1994; Fushman et al., 1994). Most commonly, a set of three different relaxation measurements, corresponding to the ^{15}N longitudinal relaxation time, T_1, its transverse relaxation time, T_2, and the heteronuclear ^{15}N-{^1H} NOE are interpreted in a model-free approach to yield an overall rotational correlation time, τ_c, and an order parameter, S^2, which is a measure for the local rigidity (Lipari and Szabo, 1982a,b).

In most previous ^{15}N relaxation studies of protein dynamics the protein has been assumed to tumble isotropically. However, Barbato et al. (1992) demonstrated that this approximation is not entirely valid for Ca^{2+}-ligated CaM, although the observed degree of anisotropy was far smaller than the anisotropy predicted for a rigid dumbbell model. In the present study, the relaxation data for Ca^{2+}-free CaM are interpreted using several different models and indicate that Ca^{2+}-free CaM behaves qualitatively similar to the Ca^{2+}-ligated form of the protein, i.e. its rotational dynamics show evidence for a limited degree of anisotropy.

MATERIALS AND METHODS

Sample preparation. Recombinant *Xenopus* calmodulin was overexpressed in *Escherichia coli* (strain AR58) containing the expression vector pTNco12. Uniform ^{15}N labeling at a level of more than 95% was obtained by growing the bacteria in M9 minimal media with $^{15}NH_4Cl$ (Isotec Inc.) as the sole nitrogen source. Protein was purified as described previously (Ikura et al., 1990). The final concentration used for this study was 1.8 mM [^{15}N]CaM in 100 mM KCl, 1.5 mM EDTA, 100 μM sodium azide, 5% D_2O, 95% H_2O, pH 6.3 in 250 μl, using a Shigemi (Shigemi Inc. Allison Park PA, USA) microcell. Addition of 1.5 mM EDTA was found to be sufficient for ligating all divalent cations; addition of more than 1.5 mM did not generate any further changes in the ^{15}N-^1H two-dimensional shift correlation NMR spectrum.

NMR spectroscopy. All experiments were performed at 23°C, using Bruker AMX-500 and AMX-600 spectrometers, each equipped with a triple-resonance 5-mm probehead containing a self-shielded z-gradient coil. The pulse sequences used for measurement of the ^{15}N T_1 and T_2 values have been adapted from those reported by Barbato et al. (1992) by including pulsed field gradients to remove unwanted coherences (Bax and Pochapsky, 1992), and by the addition of the Watergate scheme (Piotto et al., 1992) for suppressing the H_2O signal. Also, a semi-constant time evolution period (Grzesiek and Bax, 1993b) was used to optimize the acquired signal in the t_1 dimension. All experiments used States-TPPI t_1 quadrature detection in the t_1 dimension (Marion et al., 1989a).

In order to obtain independent information regarding the reproducibility of the relaxation time measurements (*vide infra*), ^{15}N T_1 measurements at 600 MHz were performed twice. A T_1 measurement was also conducted at 500-MHz ^1H frequency. Measurement of the ^{15}N T_2 values was conducted at 60.8 MHz (600 MHz ^1H frequency), both by using a CPMG-type sequence (Kay et al., 1992; Palmer et al., 1992) and by using continuous ^{15}N spin-locking with a 2.5-kHz radiofrequency field (Peng et al., 1991), i.e. effectively measuring $T_{1\rho}$. For the CPMG-type T_2 measurement, the radiofrequency field strength of the 180° pulses was 5.6 kHz, and 180° pulses were spaced 1 ms apart.

Each T_1, T_2, and $T_{1\rho}$ measurement required approximately 32 h measuring time. The ^{15}N T_1 data were acquired using ^{15}N relaxation delays of 8, 96, 200, 336, 488, 688, 968, and 1296 ms. Similarly, ^{15}N T_2 and $T_{1\rho}$ measurements were performed using relaxation delays of 8, 16, 32, 48, 64, 80, 104, and 136 ms. Each data matrix consisted of 150*×768* data points (n* denotes n complex data points), and acquisition times of 91 ms in t_1 and 83 ms in t_2 were used for each T_1 and T_2 experiment.

For measurement of the ^{15}N-{^1H} NOE, a pulse sequence which returns the H_2O magnetization to the $+z$ axis at the end of each scan was used, thereby minimizing the effect of the slowly relaxing water magnetization on the NOE measured for amides with rapidly exchanging protons (Grzesiek and Bax, 1993a). The ^{15}N-{^1H} NOE values results from the difference between two two-dimensional spectra, acquired in an interleaved manner, each consisting of a 180*×768* data matrix with acquisition times of 109 ms and 83 ms in the t_1 and t_2 dimensions, respectively. For all experiments, the ^1H carrier was positioned on the H_2O frequency and the ^{15}N carrier at 116.5 ppm. The spectral widths used were 15.4 ppm for ^1H and 27.0 ppm for ^{15}N. A repetition delay of 3 s was used for the NOE measurements. Incomplete magnetization recovery during the relaxation delay in the NOE experiment to first order can be compensated by a correction factor (Grzesiek and Bax, 1993a):

$$NOE = (1 - a)NOE_m/(1 - a \times NOE_m), \quad (1)$$

where $a = \exp(-T/T_1)$, NOE_m is the measured ratio of intensities with and without ^1H irradiation, T is the recovery delay between scans, and T_1 is the non-selective ^1H longitudinal relaxation time of the protein (≈1.4 s). This correction factor, which lowers the NOE by a small percentage relative to the measured intensity ratio, was used in determining NOE values throughout this study.

All data sets were processed using 60°-shifted squared-sine-bell filtering in both dimensions, and zero filling to 512×2048 data points. Data were processed using the program nmrPipe (F. Delaglio, unpublished) and spectra were analyzed using the software package PIPP (Garrett et al., 1991). Resonance intensities were used rather than integrated peak volumes in calculating the relaxation rates and NOE values. Note that the peak shapes for a given amide in the interleaved two-dimensional spectra are identical and the use of volume integration or peak heights in principle yields identical results except that the fractional error in volume integrals tends to be larger than for peak heights. Moreover, many of the ^1H-^{15}N correlations are insufficiently resolved to permit accurate peak integration. Errors in the derived T_1 values were estimated both by Monte-Carlo type procedures (Kamath and Shriver, 1989), which involves randomly adding or subtracting a number corresponding to the root-mean-square (rms) spectral noise from the measured intensities, and by comparing the reproducibility of T_1 values measured at 600 MHz on two separate occasions, several weeks apart. Errors in the derived T_2 values were estimated also by the Monte-Carlo procedure, and by comparing the T_2 and $T_{1\rho}$ values for the N-terminal domain of CaM. The two measurements indicated the absence of any systematic difference. The error in the NOE is estimated from assuming that the uncertainty in the peak heights in the two interleaved two-dimensional spectra, recorded with and without ^1H saturation, equals the rms noise in each of these two spectra.

Amide exchange measurements. Slowly exchanging backbone amide hydrogens were identified by dissolving a freshly

lyophilized NMR sample into 99.9% D_2O at 4°C and transferring this solution into a regular 5-mm NMR sample tube. A two-scan two-dimensional heteronuclear single quantum correlation (HSQC) experiment was started 2 min after inserting the sample into the NMR probe, thermostatted at 23°C. The time between adding D_2O to the lyophilized sample and inserting the sample into the NMR magnet was 5 min. The total duration of the HSQC measurement was also 5 min. The HSQC experiment was repeated with 8 scans/t_1 increment immediately after the first experiment was finished, i.e. 7 min after the sample temperature was raised to 23°C, and again at 63, 100 and 246 min after the sample was inserted into the magnet. After completion of the NMR experiment, its pH was measured to be 6.36, uncorrected for the deuterium isotope effect.

MODELS FOR DATA ANALYSIS

Measurement of NMR relaxation parameters such as ^{15}N T_1, T_2, and ^{15}N-{^1H} NOE are related in a direct and simple manner to spectral densities, $J(\omega)$:

$$1/T_1 = d^2 [J(\omega_H - \omega_N) + 3J(\omega_N) + 6J(\omega_H + \omega_N)] + c^2 J(\omega_N) \quad (2a)$$

$$1/T_2 = 0.5d^2 [4J(0) + J(\omega_H - \omega_N) + 3J(\omega_N) + 6J(\omega_H) + 6J(\omega_H + \omega_N)] + 1/6c^2 [3J(\omega_N) + 4J(0)] \quad (2b)$$

$$NOE = 1 + (\gamma_H/\gamma_N)\, d^2 [6J(\omega_H + \omega_N) - J(\omega_H - \omega_N)]\, T_1 \quad (2c)$$

where $d^2 = 0.1\ [(\gamma_H\ \gamma_N\ h)/(2\pi\ \langle r_{HN}^3 \rangle)]^2$ and $c^2 = 2/15\ [\omega_N^2\ (\sigma_\parallel - \sigma_\perp)^2]$, $J(\omega)$ is the spectral density function, γ_i is the gyromagnetic ratio of spin i, h is Planck's constant r_{HN} is the internuclear $^1H-^{15}N$ distance (102 pm), and $\sigma_\parallel - \sigma_\perp$ is the difference between the parallel and perpendicular components of the axially symmetric ^{15}N chemical shift anisotropy tensor, estimated at −160 ppm (Hiyama et al., 1988). Although these spectral densities are sometimes considered as the final result of a protein ^{15}N relaxation study, the intrinsic value of ^{15}N relaxation studies is to evaluate to what degree plausible physical models are either supported or contradicted by the relaxation data. Three possible models for motion of the protein are considered below: (I) isotropic tumbling of the entire protein with fast internal dynamics of limited amplitude for the individual amide N-H bond vectors, (II) axially symmetric anisotropic tumbling of the entire protein with fast internal dynamics, and (III) isotropic tumbling of the protein, with internal motions of the entire amino- and carboxy-terminal domains on an intermediate time scale, in addition to fast internal dynamics. The relation between spectral density and these models is briefly summarized below.

Isotropic model. For a protein tumbling isotropically with rotational correlation time, τ_c, and with fast internal dynamics on a time scale, τ_f, the spectral density function has the form (Lipari and Szabo, 1982a):

$$J(\omega) = S^2\tau_c/[1 + (\omega\tau_c)^2] + (1 - S^2)\,\{\tau'/[1 + (\omega\tau')^2]\} \quad (3a)$$

with

$$1/\tau' = 1/\tau_c + 1/\tau_f. \quad (3b)$$

S^2 is the generalized order parameter which describes the amplitude of the fast internal motion and assumes a value of 1 when the amplitude of the internal motion approaches zero. It is derived from the NMR data in a model-free manner but, for any given model, S^2 can be readily calculated. For example, in the commonly used model where the N-H bond vector freely diffuses in a cone of semi-angle α, S^2 is given by:

$$S^2 = [\cos\alpha\,(1 + \cos\alpha)/2]^2. \quad (4)$$

Axially symmetric model. In the Lipari-Szabo formalism (Lipari and Szabo, 1982a,b), the spectral density function for a molecule with an axially symmetric rotational diffusion tensor (Woessner, 1962a; Huntress, 1968; Hubbard, 1970) is extended to account for fast internal motions:

$$J(\omega) = S^2\,\{A_1\omega\tau_1/[1 + (\omega\tau_1)^2] + A_2\omega\tau_2/[1 + (\omega\tau_2)^2] + A_3\omega\tau_3/[1 + (\omega\tau_3)^2]\} + (1 - S^2)\,\{\tau'/[1 + (\omega\tau')^2]\} \quad (5a)$$

with

$$A_1 = 0.75 \sin^4\alpha \quad (5b)$$

$$A_2 = 3 \sin^2\alpha \cos^2\alpha \quad (5c)$$

$$A_3 = (1.5 \cos^2\alpha - 0.5)^2 \quad (5d)$$

where α is the angle between the N-H bond vector and the cylinder axis. The correlation times τ_1, τ_2, and τ_3 depend on the rotational diffusion coefficients:

$$\tau_1 = (4D_\parallel + 5D_\perp)^{-1} \quad (6a)$$

$$\tau_2 = (D_\perp + 5D_\parallel)^{-1} \quad (6b)$$

$$\tau_3 = (6D_\perp)^{-1}.$$

The time constant τ' is dominated by the time constant of the fast internal motion, τ_f. When the internal motion is at least tenfold faster than τ_1, τ_2, and τ_3, the value for τ' may be approximated by (Barbato et al., 1992):

$$1/\tau' = 1/\tau_f + 1/\tau_{c,eff} \quad (7a)$$

with

$$\tau_{c,eff} = (2D_\parallel + 4D_\perp)^{-1}. \quad (7b)$$

Both for axially symmetric and general anisotropic motion, Lipari and Szabo (1982b) have shown that $J(\omega)$, to a good approximation, can be approximated by a simpler function of the form

$$J(\omega) = S^2\,\{A\tau_1/[1 + (\omega\tau_1)^2] + (1 - A)\tau_2/[1 + (\omega\tau_2)^2]\} + A(1 - S^2)\tau'/[1 + (\omega\tau')^2] + (1 - A)\,(1 - S^2)\tau''/[1 + (\omega\tau'')^2] \quad (8a)$$

with

$$1/\tau' = 1/\tau_f + 1/\tau_1 \quad (8b)$$

$$1/\tau'' = 1/\tau_f + 1/\tau_2. \quad (8c)$$

In the case of axially symmetric motion, $J(\omega)$ is, for all practical purposes, described equally well by Eqn (8), using fewer parameters, as by Eqn (5). Similarly, the rather lengthy spectral density equation derived for the general case of anisotropic motion (Woessner, 1962b) can also be approximated by Eqn (8). However, the relation between τ_1, τ_2, and the molecular diffusion tensor can no longer be described by an equation with the simplicity of Eqn (7).

In Eqn (8), τ_1 and τ_2 are time constants that apply to the entire protein. Their magnitudes are related to the rate of tumbling and to the degree of anisotropy. For the isotropic case one has $\tau_1 = \tau_2$, and the value of A is meaningless; for axially symmetric anisotropic motion with $D_\parallel > D_\perp$, τ_1 will be slightly shorter than τ_3 of Eqn (6), and τ_2 will be slightly longer than τ_1 of Eqn (6). When applying Eqn (8) to the study of amide ^{15}N relaxation, it is important to note that, in contrast to its use by others, the value of A is not a constant for the entire protein; its value depends on the orientation of the amide N-H bond vector with respect to the molecular diffusion tensor.

Global internal motion model. The spectral density function for isotropic motion has been adapted by Clore et al.

(1990a,b) to account for cases where internal protein motions of significant amplitude occur on an intermediate time scale, τ_s ($\tau_c > \tau_s \gg \tau_f$). The spectral density function than takes on a form which is rather similar to Eqn (8):

$$J(\omega) = S^2\tau_c/[1 + (\omega\tau_c)^2] + (S_f^2 - S^2)\,\tau_s' /[1 + (\omega\tau_s')^2] + (1 - S_f^2)\tau_f'/[1 + (\omega\tau_f')^2] \quad (9)$$

with $\tau_s' = \tau_s\tau_c/(\tau_s + \tau_c)$ and $\tau_f' = \tau_f\tau_c/(\tau_f + \tau_c)$. To find the simplest description consistent with the available data, τ_f is commonly assumed to be so short that it provides a negligible contribution to $J(\omega)$, reducing Eqn (9) to two terms. For internal motions of an entire protein domain that occur on an intermediate time scale, τ_s, it is expected that the amplitude of such motions is homogeneous over the entire domain, and that all occur on the same time scale. The same approximation was made by Pastor et al. (1988) for analyzing the relaxation of methylene carbons in lipids. Thus, in contrast to the more common use of this model, we will calculate a best fit of all relaxation data to Eqn (9) using only a single value of τ_s and $S_f^2 - S^2$. Moreover, as numerous previous protein relaxation studies have shown that the order parameter (S_f^2) for residues with little ^{15}N-{^{1}H} NOE effect has a rather uniform value of about 0.85, we will fix S_f^2 at this value when searching for the values of τ_c, τ_s, and S^2. Assuming that the very fast motions are axially symmetric, an order parameter $S_s^2 = S^2/S_f^2$may be defined which is related directly to the amplitude of the slow internal motions (Clore et al., 1990a).

RESULTS AND DISCUSSION

Complete resonance assignments of the backbone amides were obtained using triple-resonance CBCA(CO)NH and CBCANH (Grzesiek et al., 1993b) experiments on a sample of uniformly ^{13}C/^{15}N-enriched CaM under conditions that are otherwise identical to those used in the present study of the internal dynamics, supplemented by information from a three-dimensional ^{15}N-separated NOE spectrum (Zuiderweg and Fesik, 1989; Marion et al., 1989b). These assignments are summarized in Table 1. The two-dimensional ^{1}H-^{15}N HSQC shift correlation map exhibits significant resonance overlap (Fig. 1), and reliable relaxation rates could only be established for 117 out of 144 observed backbone amide resonances.

T_1, T_2 and NOE data. T_1, $T_{1\rho}$, and T_2 decay data were fit to single exponentials. These data, together with the ^{1}H-{^{15}N} NOEs are presented in Table 1. The T_1 measurement at 600 MHz was repeated twice, several weeks apart, and the pairwise rms difference was 2.6% of their averaged value, indicating an rms error of 1.3% in the averaged T_1 value. Similarly, the pairwise difference between T_2 and $T_{1\rho}$ data for residues in the N-terminal half of CaM was 3% of their averaged value, suggesting an error of about 2% in the individual T_2 and $T_{1\rho}$ measurements. These errors are very similar in magnitude to the maximum deviations obtained by fitting the intensity decay multiple times, randomly adding to or subtracting from the measured peak heights a number that corresponds to the rms noise measured from a signal-free region of the corresponding spectrum. The error for the T_2 data measured at 500 MHz, obtained in this latter manner, is estimated at 2%. Analogously, an error of about 3% in the ^{1}H-{^{15}N} NOE is based on the rms noise present in the two spectra obtained with and without saturation of the ^{1}H spectrum. The relaxation data are presented graphically in Fig. 2 together with the secondary structure derived from NOE and chemical shift data (H. Kuboniwa, unpublished results). This secondary structure is very similar to that observed in Ca^{2+}-ligated CaM.

Slow conformational exchange. Comparison of ^{15}N T_2 data and $T_{1\rho}$ data, obtained with a 2.5-kHz spin lock field, show very good agreement for residues in the N-terminal half of the protein but very large differences in the C-terminal domain of the protein. Resonances with the largest difference between T_2 and $T_{1\rho}$ also exhibit, as expected, weak resonance intensity in the two-dimensional ^{15}N-^{1}H HSQC spectrum (Fig. 1). Assuming that the conformational exchange process involves two states, A and B, with populations P_A and P_B, and rate constants $k_{A\to B}$ and $k_{B\to A}$, the exchange contribution to the ^{15}N transverse relaxation time is given by (Szyperski et al., 1993)

$$1/T_2 = P_AP_B(\Delta\omega)^2\,\tau_{exch}/[1 + (\omega_1\tau_{exch})^2] + 1/T_{2,intr} \quad (10a)$$

$$\tau_{exch} = (1 - P_A)/k_{A\to B} \quad (10b)$$

where $\Delta\omega$ is the difference in angular ^{15}N chemical shift frequency between states A and B, and $T_{2,intr}$ is the intrinsic ^{15}N T_2, in the absence of conformational exchange. As the 180° pulses used during the ^{15}N T_2 relaxation delay are spaced 1 ms apart, this pulse train has an effective spin lock field strength of 500 Hz. Fitting of the observed ^{15}N T_2 rates derived from the ^{15}N line widths in the HSQC experiment and the T_2 and $T_{1\rho}$ data to Eqn (10a) yields a value for τ_{exch} of 350 ± 100 μs. Although $\Delta\omega$ is not known, it may be estimated to be at least a few ppm as even minor conformational changes frequently result in chemical shift changes of such magnitude. With this assumption, Eqn (10) yields a P_A/P_B ratio of about 25:1, i.e. a low population for one of the two conformers involved in the two-site exchange.

Hydrogen exchange. The rates of hydrogen exchange for slowly exchanging backbone amide protons were obtained by monitoring the HSQC intensity as a function of time after dissolving the protein in D_2O, and relating these intensities to those observed under the same conditions for a sample dissolved in H_2O. Considering the strong dependence of the hydrogen exchange rates on temperature, hydrogen exchange taking place during the initial sample preparation time of 300 s (at 4 °C) was not accounted for when calculating the exchange rates, but the 120 s time during which the sample temperature was raised from 4° to 23 °C (in the NMR probe) was included in full as being part of the hydrogen exchange time. The exchange time was counted until the mid-point of the data collection time. In the first HSQC spectrum, initiated 2 min after raising the sample temperature to 23 °C, 45 amides that are part of the N-terminal domain and 23 amides of the C-terminal domain could be observed, indicating exchange times longer than about 200 s, i.e. protection factors (Jeng and Englander, 1991; Bai et al., 1993) greater than ≈100. The approximate exchange rates for these amides are presented graphically in Fig. 2D. Although the slowest amide exchange is found for the first and last helix of the N-terminal domain, a substantial number of slowly exchanging amides is also present in the carboxy-terminal domain, confirming that both domains contain numerous stable hydrogen bonds.

Determination of the rotational correlation time for the isotropic motion model. For an isotropically tumbling protein, very fast internal motions on a time scale τ_f ($\tau_f \ll \omega_H^{-1}$) do not affect the T_1/T_2 ratio (cf. Eqn 2a,b), and this ratio then uniquely characterizes the rotational correlation time, τ_c, of the protein. Residues with an NOE lower than 0.6 are not used during this procedure as for such residues the condition $\tau_f \ll \omega_H^{-1}$ is clearly not valid. Although the τ_c value may be obtained from the average of the τ_c values derived individually for each residue from its T_1/T_2 ratio (Kay et al., 1989), it is better to search for

Table 1. Chemical shifts, ^{15}N relaxation times, order parameters (S^2), internal correlation times (τ_e), and hydrogen exchange rates (τ_{exch}) for the backbone amide protons in Ca^{2+}-free calmodulin. Order parameters (S^2) and internal correlation times (τ_e), were calculated using the isotropic diffusion model (cf. Eqn 3), with τ_c = 8.0 ns for residues Q3−D80, and τ_c = 7.5 ns for residues S81−K148. ^1H chemical shifts are relative to sodium 3-trimethylsilyl-(2,2,3,3-$^2H_4$)propionate TSP and ^{15}N chemical shifts are relative to liquid ammonia at 25°C. Sample conditions: 1.8 mM, pH 6.3, 100 mM KCl, 1.5 mM EDTA, 0.1 mM sodium azide, 23°C.

Residue	Shift of		$T_{1,600}$	$T_{1,500}$	$T_{2,600}$	$T_{1\rho,600}$	NOE_{600}	S^2	τ_e	τ_{exch}
	$^1H^N$	^{15}N								
	ppm		ms						ps	s
Q3	8.21	118.4	759	654	195	193	−0.004	0.629	142	< 200
L4	8.31	121.8	729	608	149	149	0.369	0.733	103	< 200
T5	8.78	112.9	665	557	109	108	0.649	0.858	76	300
E6	9.03	120.1	734	609	90	90	0.693	0.784	32	< 200
E7	8.73	119.2	727	642	82	80	0.717	0.777	25	< 200
I9	8.24	118.3	700	615	84	88	0.723	0.811	29	4 000
E11	7.80	120.1	729	612	79	79	0.690	0.792	34	1 000
F12	8.84	120.3	678	569	88	86	0.744	0.863	32	4 000
K13	9.24	121.4	690	580	85	82	0.760	0.854	24	< 200
A15	7.64	120.7	741	643	80	78	0.731	0.768	20	5 000
F16	8.54	117.8	687	582	85	86	0.754	0.847	25	5 000
S17	8.44	110.9	732	585	81	80	0.722	0.818	30	1 000
F19	7.40	114.6	736	705	85	86	0.701	0.733	23	3 000
D20	7.31	122.4	716	587	109	104	0.612	0.795	58	200
K21	8.09	123.6	756	616	126	127	0.435	0.727	80	< 200
D22	8.74	117.0	767	636	107	110	0.436	0.711	73	< 200
G23	8.02	110.3	734	626	110	106	0.569	0.751	55	< 200
D24	8.80	120.7	698	591	121	120	0.616	0.804	61	< 200
G25	10.20	111.9	649	557	104	106	0.674	0.868	69	< 200
T26	7.60	109.7	722	619	85	84	0.702	0.781	29	800
I27	8.27	110.3	669	535	75	82	0.756	0.891	34	3 000
T28	8.35	110.6	639	535	99	102	0.727	0.909	65	600
T29	8.30	112.4	688	605	88	87	0.706	0.821	36	< 200
K30	7.64	118.8	713	599	80	80	0.736	0.814	25	< 200
E31	7.52	117.4	657	537	98	98	0.712	0.894	64	500
G33	8.82	105.4	696	579	91	97	0.763	0.840	20	< 200
T34	7.53	118.3	710	614	93	90	0.757	0.810	18	< 200
V35	7.99	122.7	624	537	95	94	0.733	0.919	70	6 000
R37	8.54	119.4	687	577	85	86	0.787	0.855	13	3 000
S38	8.12	119.0	642	574	90	88	0.688	0.876	68	600
G40	7.92	107.1	769	647	87	86	0.712	0.749	22	< 200
Q41	7.78	117.7	735	632	77	79	0.740	0.784	20	500
N42	8.69	116.5	873	746	106	109	0.450	0.619	45	< 200
T44	8.80	113.2	711	599	98	96	0.715	0.810	31	200
E45	8.87	120.4	657	561	100	103	0.718	0.866	45	< 200
A46	8.34	121.0	660	560	95	94	0.689	0.865	59	2 000
L48	8.35	120.0	636	539	98	97	0.712	0.901	70	5 000
Q49	8.07	117.5	642	558	94	89	0.730	0.897	55	5 000
D50	7.85	118.9	630	532	95	93	0.764	0.922	45	800
M51	7.98	119.1	623	540	100	101	0.749	0.930	67	3 000
I52	8.35	119.0	649	518	92	93	0.736	0.912	60	6 000
N53	8.28	117.3	642	576	90	91	0.756	0.882	33	200
E54	7.59	117.3	658	557	98	100	0.674	0.867	69	< 200
V55	7.64	112.8	649	542	40	126	0.191	0.749	300	200
D56	8.48	121.9	679	577	96	96	0.677	0.836	51	< 200
A57	8.17	124.9	715	632	121	114	0.562	0.762	61	< 200
D58	8.45	114.8	719	622	117	117	0.534	0.761	68	< 200
G59	7.91	108.9	738	610	104	103	0.590	0.767	55	< 200
N60	9.29	119.8	734	627	105	106	0.606	0.768	51	< 200
T62	7.57	110.7	622	544	106	102	0.702	0.910	88	< 200
I63	8.92	118.8	683	591	94	96	0.689	0.826	43	2 000
D64	8.50	124.3	660	572	94	89	0.776	0.867	19	< 200
F65	8.66	118.6	760	625	74	77	0.711	0.759	23	500
E67	8.10	117.5	761	662	72	74	0.752	0.749	14	2 000
F68	8.49	122.4	744	626	80	82	0.763	0.783	14	10 000
T70	7.73	115.4	781	675	74	76	0.717	0.724	18	5 000
M71	7.74	121.3	727	605	72	68	0.758	0.814	18	8 000
A73	8.30	121.0	721	583	75	75	0.736	0.822	26	4 000
R74	7.47	116.8	756	699	75	72	0.679	0.720	26	600
K75	7.73	118.2	734	617	82	80	0.689	0.787	33	< 200

Table 1. Continued.

Residue	Shift of		$T_{1,600}$	$T_{1,500}$	$T_{2,600}$	$T_{1\rho,600}$	NOE_{600}	S^2	τ_e	τ_{exch}
	$^1H^N$	^{15}N								
	ppm		ms						ps	s
M76	7.96	117.8	714	604	92	93	0.614	0.777	52	< 200
D78	8.34	122.0	716	618	118	120	0.325	0.711	105	< 200
T79	8.17	114.9	737	661	121	124	0.347	0.682	84	< 200
D80	8.47	123.1	707	637	127	123	0.394	0.721	91	< 200
S81	8.48	117.2	702	608	100	110	0.569	0.770	63	< 200
E82	8.43	121.8	719	593	92	93	0.575	0.747	55	< 200
E84	8.02	119.1	696	568	69	84	0.698	0.798	34	1 000
E87	8.42	116.9	719	579	43	68	0.733	0.785	22	< 200
A88	7.51	121.3	640	530	73	87	0.769	0.869	22	600
F89	7.49	114.2	710	599	55	69	0.731	0.761	19	1 000
R90	8.25	117.9	701	602	45	71	0.752	0.787	17	< 200
V91	7.17	117.0	606	503	73	85	0.675	0.906	113	300
D93	7.84	121.3	750	650	77	80	0.701	0.720	22	< 200
K94	8.44	124.4	719	607	73	99	0.444	0.723	80	1 000
D95	8.63	116.2	645	584	76	109	0.538	0.791	86	< 200
G96	8.06	110.1	648	557	99	109	0.675	0.836	54	< 200
N97	9.02	118.7	656	575	107	113	0.644	0.823	62	< 200
Y99	7.79	118.2	631	518	68	88	0.721	0.897	62	300
S101	8.95	117.3	640	566	79	91	0.710	0.839	41	< 200
A102	8.81	124.5	669	575	80	85	0.713	0.814	33	< 200
A103	8.28	119.0	662	594	78	88	0.738	0.809	24	< 200
E104	7.75	120.2	670	527	81	92	0.683	0.846	54	700
R106	8.06	117.2	707	577	72	80	0.725	0.782	23	< 200
V108	8.14	119.5	671	574	79	80	0.664	0.808	48	300
T110	7.95	110.8	669	591	54	70	0.721	0.802	28	< 200
N111	7.65	119.8	628	568	95	98	0.627	0.824	69	< 200
L112	7.74	119.8	725	635	86	98	0.614	0.727	41	< 200
G113	8.19	108.0	664	567	135	136	0.527	0.787	87	< 200
E114	8.19	120.2	638	547	149	147	0.465	0.800	127	< 200
K115	8.27	120.1	620	574	123	136	0.454	0.798	132	< 200
L116	7.79	121.1	687	615	89	110	0.419	0.731	92	< 200
T117	8.99	113.5	652	546	108	112	0.586	0.831	92	< 200
D118	8.84	120.9	641	559	107	109	0.692	0.842	50	< 200
E119	8.59	117.9	647	523	87	99	0.667	0.853	65	< 200
E123	7.88	119.2	645	516	88	94	0.684	0.862	62	500
M124	7.91	118.7	638	530	92	97	0.647	0.852	76	500
I125	8.34	118.3	615	518	72	92	0.709	0.886	62	2 000
R126	7.96	119.6	627	521	51	75	0.693	0.871	63	900
E127	7.85	116.8	640	577	50	75	0.668	0.816	50	< 200
A128	7.60	121.5	608	520	89	97	0.664	0.893	104	300
D129	8.37	119.6	716	595	88	94	0.591	0.752	52	< 200
I130	7.85	121.0	691	586	98	99	0.562	0.766	65	< 200
D131	8.63	124.2	653	564	64	72	0.574	0.803	79	< 200
G132	8.38	107.9	653	578	96	102	0.545	0.798	88	< 200
D133	8.30	119.3	676	585	113	116	0.581	0.778	64	< 200
G134	8.54	109.5	622	541	114	114	0.599	0.856	109	< 200
Q135	8.33	119.4	688	577	108	107	0.595	0.784	62	< 200
V136	9.43	119.4	678	508	80	101	0.645	0.864	85	< 200
N137	8.81	125.1	673	553	80	94	0.684	0.819	44	< 200
Y138	7.53	122.4	586	527	87	85	0.677	0.894	94	< 200
F141	7.56	119.0	611	528	75	86	0.663	0.873	83	600
V142	8.15	120.0	647	543	92	94	0.714	0.861	47	600
M144	7.77	118.0	667	566	75	90	0.673	0.817	48	200
M145	7.99	116.0	614	533	59	86	0.649	0.873	92	< 200
T146	7.71	110.4	668	566	66	90	0.600	0.798	66	< 200
A147	7.61	125.5	649	620	118	116	0.463	0.750	89	< 200
K148	7.71	125.5	736	662	283	274	0.109	0.570	85	100

the τ_c value which minimizes the total error function, E (Dellwo and Wand, 1989):

$$E = (1/kN)\,\Sigma_N\,(T_{1,500}^{calc} - T_{1,500}^{meas})^2/(\Delta T_{1,500})^2 + (T_{1,600}^{calc} - T_{1,600}^{meas})^2/(\Delta T_{1,600})^2 + (T_2^{calc} - T_2^{meas})^2/(\Delta T_2)^2 + (NOE^{calc} - NOE^{meas})^2/(\Delta NOE)^2 \quad (12)$$

where the summation extends over all N residues with $NOE > 0.6$, and k denotes the number of measured variables

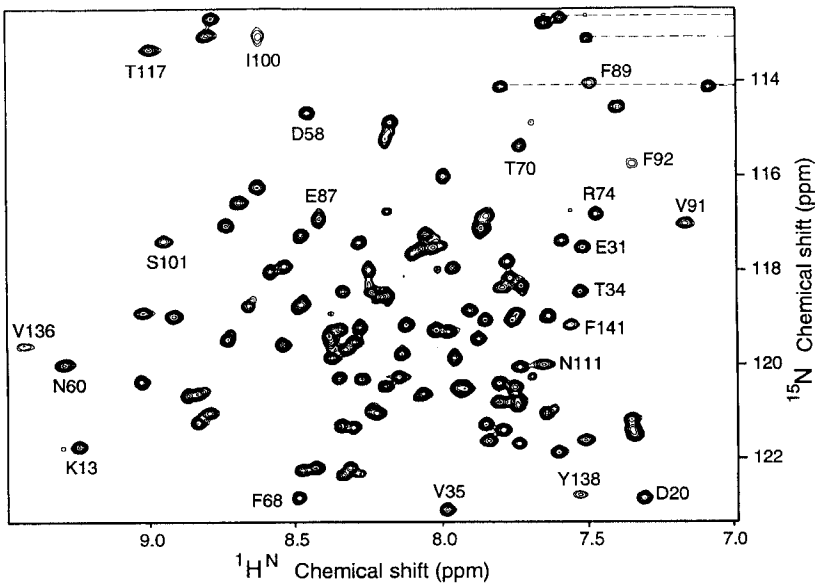

Fig. 1. A small region of the 600-MHz ^1H-^{15}N correlation spectrum of Ca^{2+}-free CaM. Horizontal dashed lines connect sidechain NH_2 resonances of Gln and Asn residues. For each of these, the second amide proton resonates outside the region shown.

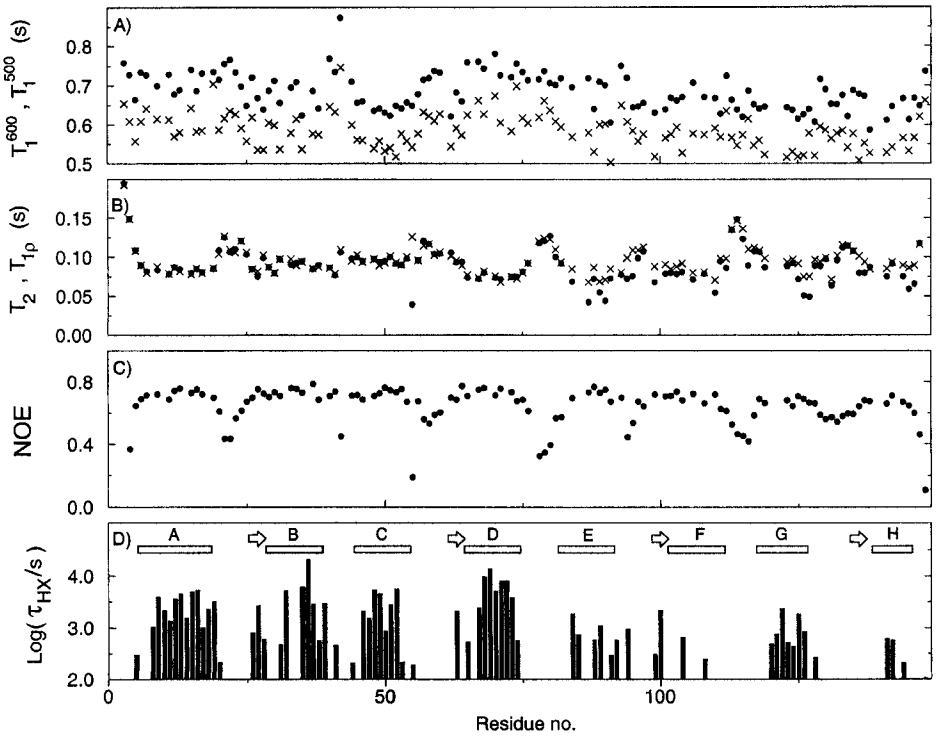

Fig. 2. Graphical representation of the relaxation data measured for Ca^{2+}-free CaM at 23°C, pH 6.3, 100 mM KCl. (A) (●) ^{15}N relaxation data measured at 60.8 MHz (600 MHz ^1H frequency) and (x) at 50.7 MHz. (B) T_2 (●) and $T_{1\rho}$ (x) data, both measured at 60.8 MHz. (C) Heteronuclear ^{15}N-{^1H} NOE, measured at 600 MHz ^1H frequency. (D) Hydrogen exchange times (τ_{HX}) and secondary structure. Open bars correspond to α-helices, open arrows correspond to the short β-strands.

used in the fit ($k = 4$, for the case where $T_{1,500}$, $T_{1,600}$, T_2, and *NOE* data were fitted). ΔT_1, ΔT_2 and ΔNOE are the standard errors in the T_1, T_2 and *NOE* measurements, the subscripts 500 and 600 (e.g. $T_{1,500}$) refer to the ^1H resonance frequency at which experiments were conducted, the superscript 'meas' refers to measured data, and 'calc' refers to the value calculated on the basis of Eqn (2), using the spectral density function of Eqn (3). Standard errors of 2% were used for the $T_{1,500}$, $T_{1,600}$, and T_2 data, and 3% for the *NOE*. In the search for the optimal τ_c value, τ_f is assumed to be zero and S^2 is allowed to vary by residue between zero and one. The last term in Eqn (12) is not used when searching for the optimal τ_c value as all reasonable values for τ_c yield NOE^{calc} values of 0.8 (using the $\tau_f = 0$ approximation). The model describes the measured data accurately if the error function approaches one. Once the value of τ_c has been determined, the search is repeated without the $\tau_f = 0$ assumption and taking the NOE term of Eqn (12) into account as well. This then yields order parameters, S^2, and τ_f values for each residue.

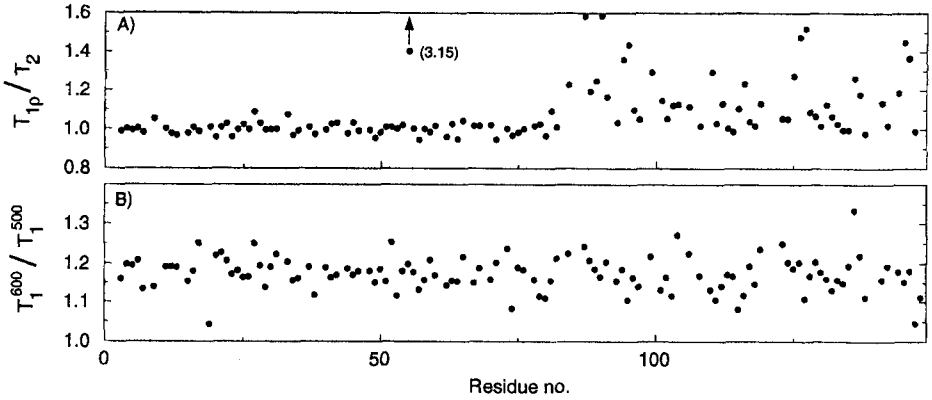

Fig. 3. Magnetic field dependence of ^{15}N relaxation times. (A) Ratio of the ^{15}N $T_{1\rho}$ and T_2 values measured at 60.8 MHz (corresponding to 600 MHz ^1H frequency). (B) Ratio of the ^{15}N T_1 values measured at 50.7 and 60.8 MHz.

N-terminal domain. For the N-terminal domain the $T_{1\rho}/T_2$ ratio is close to 1 (Fig. 3A), indicating the absence of conformational exchange processes on a time scale slower than 2.5 kHz. Moreover, the T_2 values are relatively uniform within the individual α-helices (which have their N-H bond vectors in nearly parallel orientations), suggesting that conformational exchange does not have any large effect on the measured T_2 or $T_{1\varrho}$ data. The fact that different helices show different T_2 values is related to motional anisotropy (*vide infra*), but will be ignored when attempting to derive an isotropic τ_c value. Using this approach, optimizing E for the 47 N-terminal residues which have an *NOE* larger than 0.6 yields a τ_c value of 8.4 ± 0.2 ns. The error is estimated from the largest and smallest τ_c value obtained when repeating the search 200 times, randomly omitting 15% of the measured residues for each search.

As T_2 values in the C-terminal domain are significantly shortened by a slow conformational averaging process, only T_1 and NOE data can be used for determining the apparent rotational correlation time in this domain. To demonstrate the validity of such an approach we first apply it to the N-terminal domain and demonstrate that it gives a τ_c value which is close to the value obtained with the regular procedure, used above. Previous ^{15}N relaxation studies on isotropically tumbling proteins indicate that for residues with $NOE > 0.6$, the generalized order parameter, S^2, adopts a rather uniform value of 0.85 ± 0.05. Using this assumption of a fixed $S^2 = 0.85$ value for all residues, E may be minimized using only the T_1 and NOE data. This results in a τ_c value of 7.9 ± 0.1 ns (Table 2). The fact that the error function (E) is somewhat lower compared to the case where T_1 and T_2 data are fitted does not indicate that this τ_c value is a better estimate for the rotational correlation time; it merely reflects the fact that the T_1 values and NOE data are more homogeneous than the T_2 values.

The τ_c value obtained from T_1 and NOE data is slightly shorter than the value obtained from T_1 and T_2 data. This is caused in part by the low measured NOE values, which fall in the 0.6–0.8 range, and which result in a lowering of τ_c when constraining τ_f to be zero. NOE values in this range are observed for stable regions in all previously studied proteins and reflect the fact that the $\tau_f = 0$ approximation is not entirely valid. Therefore, we also have tried to fit the T_1 data alone, again assuming $S^2 = 0.85$. This results in a τ_c value of 8.0 ± 0.1 ns (Table 2).

C-terminal domain. As mentioned above, comparison of T_2 and $T_{1\rho}$ data (Fig. 3A) suggests that T_2 values for this domain are unreliable as they are significantly affected by conformational exchange. A spin lock field considerably stronger than the 2.5 kHz used in the present study would be needed to ensure that the exchange contribution to $T_{1\rho}$ is negligible. Such strong radiofrequency fields of long durations result in unacceptable sample heating and can damage the probehead and therefore could not be used. However, as shown above, use of T_1 data alone, or of both T_1 and NOE data, yields τ_c values that are very similar to what is obtained with the more conventional approach, using T_1 and T_2 data. Using T_1 and NOE data, for all 31 residues that have $NOE > 0.6$, a τ_c value of 7.4 ± 0.2 ns is obtained. Using exclusively T_1 data results in a slightly longer τ_c value of 7.5 ± 0.1 ns (Table 2). For Ca^{2+}-ligated CaM, Barbato et al. (1992) also observed a slightly shorter τ_c value for the C-terminal domain relative to that found for the N-terminal domain, which was attributed to its number of residues.

Anisotropic model. Considering the large value of the error function E (Table 2), the isotropic model is in poor agreement with the experimental data. Also, as mentioned above, in the N-terminal domain the T_2 values are very similar within each of the four individual α-helices, but the average T_2 values for the four helices differ significantly from one another. Considering that in an α-helix, the N-H bond vectors are parallel to the helix axis, with a rms deviation of about 15°, anisotropic tumbling will cause amides within a given helix to relax rather uniformly, but amides in different helices will generally relax at different rates, depending on the orientation of the helix axis relative to the anisotropic molecular diffusion tensor. Because the structure of Ca^{2+}-free CaM has not yet been completed, it is not possible to characterize the degree of anisotropy at a detailed level. However, a lower limit for the degree of anisotropy may be estimated by considering that the T_2 values for amides in helix C are about 25% longer than for helix D. If the protein were tumbling with an axially symmetric diffusion tensor, and helices C and D were oriented perpendicular and parallel to this symmetry axis, Eqn (5) and (6) indicate that this T_2 ratio, which is dominated by $J(0)$ spectral density, corresponds to a $D_\parallel/D_\perp$ ratio of 1.6. This degree of anisotropy is larger than that previously observed for Ca^{2+}-ligated CaM at 35°C, but considerably less than the ratio of 2.5, expected from hydrodynamic calculations for a rigid dumbbell model (Barbato et al., 1992).

The α-helical backbone N-H bond vectors are not perfectly colinear with the helix axis and, on average, they make angles of about 15° with this axis. Assuming axially symmetric anisotropic diffusion, the amide in helix D which has the longest T_2 value (F68, 81 ms) is expected to make an angle with the unique axis of the diffusion tensor that is ≈15° larger than the angle between the unique axis and helix D. Similarly, the amide of

Table 2. Correlation times and values for the error function, *E*, derived for the N- and C-terminal domains of Ca^{2+}-free CaM at 23°C, assuming isotropic motion. The error function, *E*, extends only over the input parameters used. Uncertainties correspond to the maximum deviation when repeating the search 200 times, omitting randomly 15% of the residues. *N* and *p* are the number of residues and the number of variables used in the fitting procedure.

Input parameters	Domain	τ_c	*E*	*N*	*p*
		ns			
$T_{1,600}$; $T_{1,500}$; $T_{2,600}$; $T_{1\rho,600}$	N	8.4 ± 0.2	19 ± 3	47	48
$T_{1,600}$; $T_{1,500}$; *NOE*	N	7.9 ± 0.1	15 ± 2	47	1
$T_{1,600}$; $T_{1,500}$	N	8.0 ± 0.1	16 ± 2	47	1
$T_{1,600}$; $T_{1,500}$; *NOE*	C	7.4 ± 0.2	16 ± 2	31	1
$T_{1,600}$; $T_{1,500}$	C	7.5 ± 0.1	18 ± 2	31	1

Q49 in helix D which has the shortest transverse relaxation rate (91 ms) is expected to make an angle with the unique axis which is ≈15° smaller than the angle between this axis and helix C. Considering that the fastest relaxing amide in helix C relaxes considerably slower than the slowest relaxing amide in helix D, the angle between helix D and the unique axis must be smaller by significantly more than 30° compared to the angle between the unique axis and helix C. The angle between helices C and D is therefore also significantly larger than 30°. Helices A and B, which exhibit ^{15}N T_2 values intermediate between those of helices C and D, must make angles with the unique axis of the diffusion tensor that fall between those of helices C and D. Note that small non-uniformity of the order parameter, S^2, and/or small random errors in the T_2 measurements statistically bring the shortest T_2 value in helix C and the longest T_2 value in helix D closer to one another, and the above analysis of the minimum angle between helices C and D is therefore very conservative.

In the Ca^{2+}-free N-terminal domain of troponin C, helices C and D have an interhelix angle of 146°, whereas helix D makes angles of 115° and 53° with helices A and B, respectively (Strynadka and James, 1989). In Ca^{2+}-ligated CaM these angles are 84° (C/D), 115° (A/D) and 34° (B/D). Herzberg et al. (1986) proposed that binding of calcium is responsible for the large difference in helical angles between the Ca^{2+}-free N-terminal domain of troponin C and its Ca^{2+}-ligated C-terminal domain. Strynadka and James (1988) suggest that Ca^{2+}-free CaM adopts a similar helical arrangement as observed in the N-terminal domain of troponin C, with a C/D angle of 151°. However, as argued above, an angle of 151° (equivalent to 180°−151° = 29°, from an NMR relaxation viewpoint) appears incompatible with the rather large difference in transverse relaxation rates observed for amides in helices C and D, suggesting that at a quantitative level the Strynadka and James model may not be quite accurate.

Global internal motion model. Both for the isotropic and anisotropic tumbling models, it is readily seen that in the motional correlation time range applicable for CaM (>5 ns), T_1 values at 600 MHz ^1H frequency are expected to be longer than T_1 values at 500 MHz by approximately the ratio of the corresponding spectral densities, $J(2\pi\times51\times10^6)/J(2\pi\times61\times10^6)$. Taking into account the increase in chemical shift anisotropy at the higher field (expressed in Hertz), a $T_{1,600}/T_{1,500}$ ratio of about 1.28 is expected. Indeed, this is very close to the average ratio previously found for staphylococcal nuclease (Kay et al., 1989) ($\tau_c \approx 9$ ns). However, the $T_{1,600}/T_{1,500}$ ratios observed for Ca^{2+}-free CaM are considerably smaller than 1.28 (Fig. 3B) and have an average ratio of only 1.18. This smaller than anticipated $T_{1,600}/T_{1,500}$ ratio cannot be explained by motional anisotropy because the low value is observed throughout the protein. Note that in a model of a protein tumbling with an axially symmetric diffusion tensor the amides oriented along the cylinder axis relax at the same rate as in a protein isotropically tumbling with a correlation time, $\tau_c = 1/(6D_\perp)$. So, regardless of $D_\parallel$, at least for helix *D* one would expect a $T_{1,600}/T_{1,500}$ ratio close to 1.28, in contrast to what is observed. A second indication that the smaller than expected $T_{1,600}/T_{1,500}$ ratio is not caused by motional anisotropy is the fact that the degree of anisotropy in the T_1 values is considerably less than what is observed for the T_2 values.

These observations can be explained by assuming that the entire N-terminal domain undergoes large amplitude motions on a time scale that significantly shortens the ^{15}N T_1 values relative to that of a slowly tumbling rigid dumbbell. Previously, Clore et al. (1990a, b) proposed one should use the extended spectral density function of Eqn (9) to account for such motions. When using this equation, τ_c is typically fixed at a constant value which is determined from residues with relaxation times that can be fit with the simple Lipari-Szabo spectral density function of Eqn (3), and S_f^2, S^2 and the correlation time for slow internal motion, τ_s, are optimized for each residue individually. In the present case, where an entire protein domain is subject to motion on an intermediate time scale, τ_s is expected to be the same for all residues and the order parameter for this motional process, S_s^2, is also expected to be uniform. In addition, as argued above, a S_f^2 value of 0.85 is commonly observed in proteins for residues with a ^{15}N-{^1H} NOE larger than 0.6. Therefore, we have searched for the τ_c, τ_s, and S^2 values that optimize the fit between Eqn (9) and the observed $T_{1,600}$, $T_{1,500}$, T_2, $T_{1\rho}$ and NOE data. The results of these searches are summarized in Table 3 where it can be seen that this extended model provides a considerably better fit to the experimental data than does the simple isotropic tumbling model (Table 2). The global internal motion model suggests an overall correlation time, τ_c, in the 10−13-ns range, with internal motions of the two individual domains on a time scale of ≈3 ns. An internal correlation time of 3 ns is reasonable considering that small proteins the size of a single CaM domain are expected to tumble on this time scale (Peng and Wagner, 1992; Akke et al., 1993; Barchi et al., 1994).

The global internal motion as used in the present study is clearly oversimplified as it does not include the effects of anisotropy of the overall protein motion. The slow overall tumbling contributes relatively little to T_1 relaxation, but dominates T_2 relaxation and causes a pronounced dependence of the T_2, observed for a given amide, on the orientation of the N-H bond vector relative to the principal axes of the overall diffusion tensor. Therefore, this model cannot account for the noticible anisotropy in the ^{15}N T_2 values, mentioned above, and the error function remains large when the T_2 data is included in the fitting procedure (Table 3). A model which includes the effect of

Table 3. Global rotational correlation time (τ_c), and correlation time (τ_s) for the rigid body domain motions of the N- and C-terminal domains of Ca^{2+}-free CaM at 23°C, obtained using the extended spectral density function of Eqn (9), and assuming $\tau_f = 0$. The generalized order parameter (S^2) includes the effects of motion on the τ_s time scale and of very fast ($\tau_f \approx 0$) internal motions, described by a uniform order parameter, $S_f^2 = 0.85$. The error function, E, extends only over the input parameters used. Uncertainties correspond to the maximum deviations when repeating the search 200 times, omitting randomly 15% of the residues. N and p are the number of residues and the number of variables used in the fitting procedure.

Input parameters	Domain	τ_c	τ_s	S^2	E	N	p
		ns					
$T_{1,600}$; $T_{1,500}$; $T_{2,600}$; $T_{1\rho,600}$	N	12.0 ± 0.4	2.8 ± 0.2	0.56 ± 0.03	15 ± 4	47	3
$T_{1,600}$; $T_{1,500}$; *NOE*	N	12.8 ± 0.5	2.8 ± 0.2	0.56 ± 0.02	8 ± 2	47	3
$T_{1,600}$; $T_{1,500}$	N	13.6 ± 1	3.4 ± 0.9	0.53 ± 0.04	10 ± 4	47	3
$T_{1,600}$; $T_{1,500}$; *NOE*	C	9.6 ± 0.5	2.2 ± 0.2	0.60 ± 0.02	7 ± 2	31	3
$T_{1,600}$; $T_{1,500}$	C	10.6 ± 0.5	2.8 ± 0.4	0.57 ± 0.3	9 ± 3	31	3

anisotropy of the overall motion requires knowledge of the orientation of each of the N-H bond vectors within each of calmodulin's domains and therefore cannot be used in the present case.

The value for $S^2 \approx 0.56$ corresponds to a value of $S_s^2 = S^2/S_f^2 = 0.66$. The assumption of restricted diffusion of the individual domains in a cone of semi-angle α may be used to obtain an approximate idea regarding the magnitude of these motions. Use of Eqn (4) indicates a value for α of ≈30°. Considering that both domains would freely diffuse in their own cones, the maximum angular excursion of one domain relative to the other one would be approximately 60° in such a model. Indeed, the linker between helices D and E, extending over residues M76–S81 is found to exhibit considerable flexibility, with T_2 values that are nearly 50% longer compared to helices D and E. The ^{15}N-{^1H} NOE values for these residues also drop to low values which is characteristic of high flexibility, indicating that these residues serve as the flexible tether between the two domains, completely analogous to that which was observed previously for Ca^{2+}-ligated CaM (Barbato et al., 1992), except that the residual degree of anisotropy is somewhat larger in the present case.

CONCLUSIONS

In the absence of calcium, CaM adopts a well-folded structure with numerous slowly exchanging backbone amide protons. Its dynamics cannot adequately be described by a model of an isotropically tumbling protein with fast, small, amplitude internal motions. In particular, the ^{15}N T_1 data measured at 51 and 61 MHz ^{15}N frequency are incompatible with a model of a rigid protein tumbling anisotropically. Significantly better agreement with the measured relaxation data is obtained in a model where the individual domains have restricted mobility on a time scale of about 3 ns, superimposed on the overall tumbling of the molecule which occurs on a time scale which is about 4 times slower. Residues M76–S81 are located between helix D of the N-terminal domain and helix E, the first helix of the C-terminal domain. These residues show relaxation behavior characteristic of a flexible linker. In the simplest of models, where each entire domain is subject to restricted diffusion in a cone of semi-angle α, the ^{15}N relaxation data are compatible with α values of ≈30°, corresponding to a maximum fluctuation of ±60° in the relative orientations of helices D and E.

Hydrogen exchange data indicate that, on average, the N-terminal domain is more stable than the C-terminal domain, confirming an earlier report on the melting behavior of the individual domains (Brzeska et al., 1983). However, slowly exchanging amide protons are observed in all eight α-helices and in three of the four short β-strands, indicating that these all form well-defined hydrogen-bonded structures. Substantial line broadening of many of the ^{15}N resonances in the C-terminal domain is caused by conformational exchange, on a time scale of a few hundred microseconds. At the temperature where the present dynamics study was conducted (23°C), one of the two conformers has a low population (<10%). There is no correlation between the extent to which the ^{15}N relaxation time of the individual C-terminal residues is affected by conformational exchange and the rates at which the backbone amides exchange with solvent. It is therefore unlikely that the conformational exchange process is the cause for the faster hydrogen exchange in the C-terminal domain relative to that observed in the N-terminal domain. Considering that the conformational exchange occurs on the same time scale for all C-terminal residues affected by this process, it is also unlikely that the ^{15}N broadening is the result of several independent conformational changes.

The overall tumbling of Ca^{2+}-free CaM is somewhat slower and noticeably more anisotropic than for Ca^{2+}-ligated CaM (Barbato et al., 1992). However, this difference is caused in part by the difference in temperature at which the two forms of the protein were studied. In fact, when studying the temperature dependence of the dynamics of Ca^{2+}-ligated CaM, we found that, at the same temperature, the Ca^{2+}-ligated form of the protein actually tumbles slower and with a similar degree of anisotropy as the Ca^{2+}-free form (Do, R. et al., unpublished results). This is in agreement with small-angle X-ray scattering results which indicate a smaller maximum length vector for the Ca^{2+}-free form (Yoshino et al., 1989; Heidorn and Trewhella, 1988).

The large difference in transverse ^{15}N relaxation rates observed for amides in helix C versus those in helix D appears incompatible with the nearly antiparallel arrangement of these helices in the model for Ca^{2+}-free CaM proposed by Strynadka and James (1988). This finding suggests that their troponin-C-based model of the calcium-dependent conformational switch may need refinement. A definitive answer to this question is expected from the determination of the Ca^{2+}-free CaM structure, presently in progress.

We thank Claude B. Klee for continuous encouragement, Stephan Grzesiek for assistance in recording the relaxation data, Frank Delaglio and Dan Garrett for the development of software for facilitating the data analysis, Richard Do for performing the study of the temperature dependence of Ca^{2+}-ligated CaM, Andy Wang for many useful suggestions during the preparation of the manuscript and Attila Szabo and Dennis Torchia for numerous enlightening and stimulating discussions. This work was supported by the AIDS Targeted Anti-Viral Program of the Office of the Director of the National Institutes of Health. NT acknowl-

edges support from a National Institute of Diabetes and Digestive and Kidney Diseases/National Research Society for Arthritis grant (1F32DK09143-01).

REFERENCES

Akke, M., Skelton, N. J., Kordel, J., Palmer, A. G. & Chazin, W. J. (1993) *Biochemistry 32*, 9832–9844.

Alexandrescu, A. T. & Shortle, D. (1994) *J. Mol. Biol. 242*, 527–546.

Babu, Y. S., Sack, J. S., Greenhough, T. J., Bugg, C. E., Means, A. R. & Cook, W. J. (1985) *Nature 315*, 37–40.

Babu, Y. S., Bugg, C. E. & Cook, W. J. (1988) *J. Mol. Biol. 204*, 191–204.

Bai, Y., Milne, J. S., Mayne, L. & Englander, S. W. (1993) *Proteins, Struct. Funct. Genet. 17*, 75–86.

Barbato, G., Ikura, M., Kay, L. E., Pastor, R. W. & Bax, A. (1992) *Biochemistry 31*, 5269–5278.

Barchi, J. J., Grasberger, B., Gronenborn, A. M. & Clore, G. M. (1994) *Protein Sci. 3*, 15–21.

Bax, A. & Pochapsky, S. (1992) *J. Magn. Reson. 99*, 638–643.

Brzeska, H., Venyaminov, S. V., Grabarek, Z. & Drabikowski, W. (1983) *FEBS Lett. 153*, 169–173.

Clore, G. M., Szabo, A., Bax, A., Kay, L. E., Driscoll, P. C. & Gronenborn, A. M. (1990a) *J. Am. Chem. Soc. 112*, 4989–4991.

Clore, G. M., Driscoll, P. C., Wingfield, P. T. & Gronenborn, A. M. (1990b) *Biochemistry 29*, 7387–7401.

Cohen, P. & Klee, C. B. (1988) *Calmodulin*, Elsevier, New York.

Dellwo, M. J. & Wand, A. J. (1989) *J. Am. Chem. Soc. 111*, 4571–4578.

Finn, B. E., Drakenberg, T. & Forsen, S. (1994) *FEBS Lett. 336*, 368–374.

Fushman, D., Ohlenschlager, O. & Rüterjans, H. (1994) *J. Biomol. Struct. Dyn. 11*, 1377–1402.

Garrett, D. S., Powers, R., Gronenborn, A. M. & Clore, G. M. (1991) *J. Magn. Reson. 94*, 214–220.

Grzesiek, S. & Bax, A. (1993a) *J. Am. Chem. Soc. 115*, 12593–12594.

Grzesiek, S. & Bax, A. (1993b) *J. Biomol. NMR 3*, 185–204.

Heidorn, D. B. & Trewhella, J. (1988) *Biochemistry 27*, 909–915.

Herzberg, O. & James, M. N. G. (1988) *J. Mol. Biol. 203*, 761–779.

Herzberg, O., Moult, J. & James, M. N. G. (1986) *J. Biol. Chem. 261*, 2638–2644.

Hiyama, Y., Niu, C., Silverton, J. V., Bavoso, A. & Torchia, D. A. (1988) *J. Am. Chem. Soc. 110*, 2378–2383.

Hubbard, P. S. (1970) *J. Chem. Phys. 52*, 563–568.

Huntress, W. T. (1968) *J. Chem. Phys. 48*, 3524–3533.

Ikura, M., Marion, D., Kay, L. E., Shih, H., Krinks, M., Klee, C. B. & Bax, A. (1990) *Biochem. Pharmacol. 40*, 153–160.

Ikura, M., Clore, G. M., Gronenborn, A. M., Zhu, G., Klee, C. B. & Bax, A. (1992) *Science 256*, 632–638.

Jeng, M.-F. & Englander, S. W. (1991) *J. Mol. Biol. 221*, 1045–1061.

Kamath, U. & Shriver, J. W. (1989) *J. Biol. Chem. 264*, 5586–5592.

Kay, L. E., Nicholson, L. K., Bax, A. & Torchia, D. A. (1992) *J. Magn. Reson. 97*, 359–375.

Kay, L. E., Torchia, D. A. & Bax, A. (1989) *Biochemistry 28*, 8972–8979.

Lipari, G. & Szabo, A. (1982a) *J. Am. Chem. Soc. 104*, 4546–4558.

Lipari, G. & Szabo, A. (1982b) *J. Am. Chem. Soc. 104*, 4559–4570.

Marion, D., Ikura, M., Tschudin, R. & Bax, A. (1989a) *J. Magn. Reson. 85*, 393–399.

Marion, D., Kay, L. E., Sparks, S. W., Torchia, D. A. & Bax, A. (1989b) *J. Am. Chem. Soc. 111*, 1515–1517.

Meador, W. E., Means, A. R. & Quiocho, F. A. (1992) *Science 257*, 1251–1255.

Meador, W. E., Means, A. R. & Quiocho, F. A. (1993) *Science 262*, 1718–1721.

Orekhov, V. Y., Pervushin, K. V. & Arseniev, A. S. (1994) *Eur. J. Biochem. 219*, 887–896.

Palmer, A. G. (1993) *Curr. Opin. Biotechn. 4*, 385–391.

Palmer, A. G., Skelton, N. J., Chazin, W. J., Wright, P. E. & Rance, M. (1992) *Mol. Phys. 75*, 699–711.

Pastor, R. W., Venable, R. M., Karplus, M. & Szabo, A. (1988) *J. Chem. Phys. 88*, 1128–1140.

Peng, J. W. & Wagner, G. (1992) *Biochemistry 31*, 8571–8586.

Peng, J. W. & Wagner, G. (1994) *Methods Enzymol. 239*, 563–596.

Peng, J. W., Thanabal, V. & Wagner, G. (1991) *J. Magn. Reson. 94*, 82–100.

Piotto, M., Saudek, V. & Sklenar, V. (1992) *J. Biomol. NMR 2*, 661–665.

Redfield, C., Boyd, J., Smith, L. J., Smith, R. A. G. & Dobson, C. M. (1992) *Biochemistry 31*, 10431–10437.

Schneider, D. M., Dellwo, M. J. & Wand, A. J. (1992) *Biochemistry 31*, 3645–3652.

Strynadka, N. C. & James, M. N. G (1988) *Proteins Struct. Funct. Genet. 3*, 1–17.

Strynadka, N. C. J. & James, M. N. G. (1989) *Annu. Rev. Biochem. 58*, 951–998.

Sundaralingam, M., Bergstrom, R., Strasburg, S., Rao, S. T., Roychowdhury, M., Greaser, M. & Wang, B. C. (1985) *Science 227*, 945–948.

Szyperski, T., Luginbühl, P., Otting, G. & Wüthrich, K. (1993) *J. Biomol. NMR 3*, 151–164.

Taylor, D. A., Sack, J. S., Maune, J. F., Beckingham, K. & Quiocho, F. A. (1991) *J. Biol. Chem. 266*, 21375–21380.

Torchia, D. A., Nicholson, L. K., Cole, H. B. R. & Kay, L. E. (1993) *NMR of proteins* (Clore, G. M. & Gronenborn, A. M., eds) pp. 190–219, MacMillan, London.

van Mierlo, C. P., Darby, N. J., Keeler, J., Neuhaus, D. & Creighton, T. E. (1993) *J. Mol. Biol. 229*, 1125–1146.

Wagner, G., Hyberts, S. & Peng, J. W. (1993) *NMR of proteins* (Clore, G. M. & Gronenborn, A. M., eds) pp. 220–257, MacMillan, London.

Woessner, D. T. (1962a) *J. Chem. Phys. 37*, 647–654.

Woessner, D. T. (1962b) *J. Chem. Phys. 36*, 1–4.

Yoshino, H., Minari, O., Matsushima, N., Ueki, T., Miyake, Y., Matsuo, T. & Izumi, Y. (1989) *J. Biol. Chem. 264*, 19706–19709.

Zuiderweg, E. R. P. & Fesik, S. W. (1989) *Biochemistry 28*, 2387–2391.

Note added in proof: Preliminary NMR structure calculations for Ca^{2+}-free calmodulin indicate a C/D angle of 125°.